Cell Reports

Article

HCAR1/MCT1 Regulates Tumor Ferroptosis through the Lactate-Mediated AMPK-SCD1 Activity and Its Therapeutic Implications

Graphical Abstract

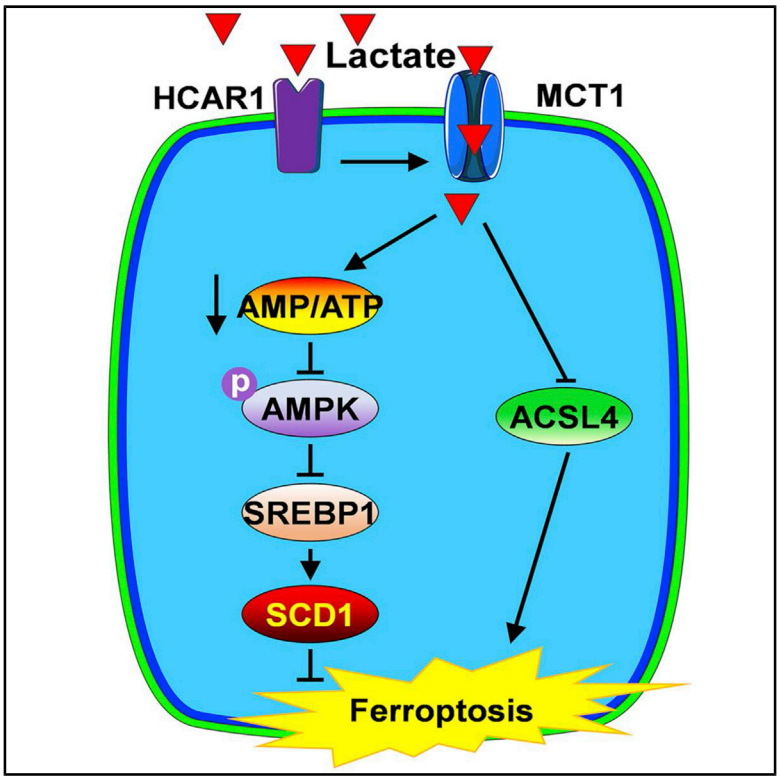

Highlights

- Lactate uptake promotes ATP production to upregulate SREBP1 and SCD1
- Lactate mediates the production of ferroptosis-related lipids in cancer cells
- HCAR1/MCT1 inhibition sensitizes cancer cells to ferroptosis induction

Authors

Youbo Zhao, Menghuan Li, Xuemei Yao, ..., Kaiyong Cai, Yanli Zhao, Zhong Luo

Correspondence

luozhong918@cqu.edu.cn

In Brief

Zhao et al. discover a lactate-mediated ferroptosis regulatory pathway in liver cancer cells, through which lactate enhances their ferroptosis resistance by upregulating the production of anti-ferroptosis monounsaturated fatty acids. Their findings may provide avenues for the development of ferroptosis-based cancer therapies.

Zhao et al., 2020, Cell Reports *33*, 108487
December 8, 2020
https://doi.org/10.1016/j.celrep.2020.108487

CellPress

Cell Reports

CellPress
OPEN ACCESS

Article

HCAR1/MCT1 Regulates Tumor Ferroptosis through the Lactate-Mediated AMPK-SCD1 Activity and Its Therapeutic Implications

Youbo Zhao,[1,4] Menghuan Li,[1,4] Xuemei Yao,[1] Yang Fei,[1] Zhenghong Lin,[1] Zhengguo Li,[1] Kaiyong Cai,[2] Yanli Zhao,[3] and Zhong Luo[1,*]

[1]School of Life Science, Chongqing University, Chongqing 400044, China
[2]Key Laboratory of Biorheological Science and Technology, Ministry of Education, College of Bioengineering, Chongqing University, Chongqing 400044, China
[3]Division of Chemistry and Biological Chemistry, School of Physical and Mathematical Sciences, Nanyang Technological University, 21 Nanyang Link, Singapore 637371, Singapore
[4]These authors contributed equally
*Correspondence: luozhong918@cqu.edu.cn
https://doi.org/10.1016/j.celrep.2020.108487

SUMMARY

Ferroptosis is a recently discovered form of programed cell death caused by the metabolically regulated lipid peroxidation and holds promise for cancer treatment, but its regulatory mechanisms remain elusive. In this study, we observe that lactate-rich liver cancer cells exhibit enhanced resistance to the ferroptotic damage induced by common ferroptosis inducers such as Ras-selective lethal small molecule 3 (RSL3) and Erastin and that the monocarboxylate transporter 1 (MCT1)-mediated lactate uptake could promote ATP production in hepatocellular carcinoma (HCC) cells and deactivate the energy sensor AMP-activated protein kinase (AMPK), leading to the upregulation of sterol regulatory element-binding protein 1 (SREBP1) and the downstream stearoyl-coenzyme A (CoA) desaturase-1 (SCD1) to enhance the production of anti-ferroptosis monounsaturated fatty acids. Additionally, blocking the lactate uptake via hydroxycarboxylic acid receptor 1 (HCAR1)/MCT1 inhibition promotes ferroptosis by activating the AMPK to downregulate SCD1, which may synergize with its acyl-coenzyme A synthetase 4 (ACSL4)-promoting effect to amplify the ferroptotic susceptibility. *In vitro* and *in vivo* evidence confirms that lactate regulates the ferroptosis of HCC cells and highlights its translational potential as a therapeutic target for ferroptosis-based tumor treatment.

INTRODUCTION

Despite the recent advances in the development of treatment modalities for various cancer indications, liver cancer still remains one of the leading causes of death worldwide and poses a grave threat to human health (Chen et al., 2016a; Craig et al., 2020; Siegel et al., 2020). Most of the conventional anticancer drugs rely on apoptosis induction to exert therapeutic effects (Ma et al., 2017; Su et al., 2018), but their efficacy is usually limited due to the intrinsic or acquired apoptosis resistance in the clinical context. Therefore, new therapeutic avenues based on alternative cell death mechanisms are under constant investigation to enhance the eventual treatment outcome. Among these emerging cell death mechanisms, ferroptosis is one such candidate that has shown promise for clinical translation (Ingold et al., 2018; Shen et al., 2018; Song et al., 2018; Zhang et al., 2018; Zou and Schreiber, 2020). Ferroptosis is a non-apoptotic form of regulated cell death characterized by the accumulation of cytotoxic lipid reactive oxygen species (ROS), which would ultimately lead to lethal lipid membrane damage and perforation (Dixon and Stockwell, 2019; Fang et al., 2019; Gaschler et al., 2018; Hassannia et al., 2019; Murphy, 2018). Considering the central role of lipid peroxidation in the ferroptosis process, it has been increasingly recognized that the lipid composition in cancer cells could have profound impact on their sensitivity to ferroptosis-inducing agents. Typically, previous insights collectively demonstrate that the ferroptosis process is driven by the peroxidation of oxidizable polyunsaturated fatty acids (PUFAs), of which the biosynthesis is catalyzed by the acyl-coenzyme A (CoA) synthetase (ACSL4) (Conrad and Pratt, 2019; Doll et al., 2017). It has also been reported that the stearoyl-CoA desaturase-1 (SCD1)-catalyzed monounsaturated fatty acids (MUFAs) may potently inhibit ferroptosis by replacing PUFAs in the lipid membrane and reducing the accumulation of lipid ROS thereof (Das, 2019; Magtanong et al., 2019; Tesfay et al., 2019). Nevertheless, the endogenous mechanism that may affect the lipid-mediated ferroptosis resistance is still unclear, which would be relevant to the development of new ferroptosis-based therapies with enhanced clinical efficacy.

A common feature among various cancer cells is that their metabolic pathways are rewired to aerobic glycolysis to facilitate cancer cell survival and growth (Kim and DeBerardinis, 2019),

whereas lactate is the main metabolic product. Nevertheless, increasing evidence reveals that lactate is not a mere metabolic waste but a nutrient (Faubert et al., 2017; Hui et al., 2017) that has many regulatory roles in the tumor microenvironment, and it demonstrates particular relevance to oxidative stress resistance (Tasdogan et al., 2020; Tauffenberger et al., 2019) and lipid biosynthesis (Chen et al., 2016b). For instance, it has been confirmed that extracellular lactate is not only one of the major carbon sources for lipid biosynthesis but also could regulate the production of various lipid substances via AMP-activated protein kinase (AMPK) or signal transducer and activator of transcription 3 (STAT3) signaling (Pucino et al., 2019). However, despite the strong evidence for the involvement of lactate in the membrane lipid landscape, it is still unclear whether the extracellular lactate could regulate the cancer cell response to ferroptosis induction by small-molecule agents. In fact, it has already been reported that hepatocellular carcinoma (HCC) demonstrated high resistance to Sorafenib via the SCD1-mediated endoplasmic reticulum (ER) stress inhibition (Ma et al., 2017), which is a Food and Drug Administration-approved anticancer drug with clinically tested ferroptosis-inducing capabilities. Therefore, we hypothesize that lactate may enhance the ferroptosis resistance in cancer cells by leveraging the production of ferroptosis-related lipids and that inhibiting MCT1 and its receptor HCAR1 may contribute to the tumor suppression effect of ferroptosis-based treatments.

Clinical investigations have collectively revealed that the expression level of HCAR1 is low in normal hepatocytes. By comparison, the HCAR1 expression has been significantly upregulated in HCC cells. This is also consistent with our assessment on the expression levels of HCAR1 in patient-derived HCC samples via qPCR and western blot. Moreover, the upregulated MCT1 and HCAR1 levels are correlated with increasing resistance to the ferroptotic damage induced by typical ferroptosis inducers such as RSL3, Erastin, and Sorafenib. To further elucidate the regulatory role of lactate in the ferroptosis process of HCC cells, we examined the regulatory cascade of lactate *in vitro* and *in vivo* and observed that increasing lactate concentration in the tumor microenvironment could activate the HCAR1 receptors on the cytoplasmic membrane of HCC cells and facilitate the MCT1-mediated uptake of lactate, which would enhance the ATP production and lower the AMP:ATP ratio in the intracellular compartment. The lactate-induced disruption of AMP:ATP balance would further deactivate AMPK to downregulate the expression of the sterol regulatory element-binding protein 1 (SREBP1) and its target SCD1, thus increasing the production of anti-ferroptosis MUFAs and inhibiting lipid peroxidation. We also observed that blocking lactate uptake via HCAR1/MCT1 inhibition may suppress the ACSL4-mediated production of pro-ferroptosis PUFAs, leading to synergistic ferroptosis-sensitizing effect. Considering the low HCAR1/MCT1 expression level in normal liver cells, HCAR1 and MCT1 could present highly specific targets for ferroptosis-based therapy against HCC. To evaluate the therapeutic potential of HCAR1/MCT1 inhibition, we blocked the cross-membrane lactate transport in HCC cells via HCAR1/MCT1 knockdown or AZD3965 (MCT1 inhibitor) treatment and observed that these treatments could drastically enhance the sensitivity of HCC cells to the ferroptosis effect induced by RSL3 and Sorafenib, leading to markedly increased HCC inhibition effect *in vitro* and *in vivo*. Overall, this study identified that lactate in the tumor microenvironment is a negative regulator driving ferroptosis resistance, which may serve as a potential therapeutic target to improve the efficacy of ferroptosis-based therapies.

RESULTS

Liver Cancer Cells with Elevated Extracellular Lactate Levels Develop Resistance to Ferroptosis-Based Therapy

As discussed above, the lactate level in the HCC extracellular environment is often aberrantly upregulated due to the glycolysis. Therefore, to mimic the high extracellular lactate level of HCC in real-life conditions and investigate its potential impact on the response of HCC cells to ferroptosis, we added lactate into the culture media of Hep3B and Huh-7 cells and then treated them with two ferroptosis-inducing agents, RSL3 and Erastin. According to previous reports, the lactate level in normal tissues was as low as 1.3 mM, while that in the tumor tissues has been significantly elevated to ~10–40 mM. Consequently, the lactate concentration for the *in vitro* experiments in this study was fixed at 20 mM by referring to the experimental setup in previous reports (Harmon et al., 2019; Roland et al., 2014). As demonstrated by the cell viability analysis in Figure 1A and Figure S1A, the survival rate of Hep3B and Huh-7 cells was as low as 43% and 38.9%, respectively, when treated with only RSL3, and increased to 81.2% and 80% when treated with lactate and RSL3. It could be observed that both types of liver cancer cells showed enhanced resistance to the ferroptotic cell death induced by RSL3 and Erastin and that the difference was statistically significant, supporting the potential role of lactate as a negative ferroptosis regulator in HCC cells. In addition to direct lactate supplementation, we also prepared carcinoma-associated fibroblasts (CAFs)-conditioned medium (CM) with elevated lactate levels for culture of liver cancer cells (Figures S1B–S1D) and then monitored their response to RSL3 and Erastin treatment. CAF is one of the most abundant components in tumor stroma and also a major source of lactate in the extracellular environment (Ippolito et al., 2019b). Consequently, it is anticipated that the CM would present close resemblance to the actual lactate-rich tumor microenvironment in HCC-bearing patients. According to the cell survival assays, both Hep3B and Huh-7 cells cultured in CM showed reduced susceptibility to the ferroptosis effects induced by RSL3 and Erastin in comparison with those incubated in pristine DMEM media (Figure 1B; Figure S1E). Consistent with the experimental results using RSL3 and Erastin, we found that the treatment with additional exogenous lactate or CM has enhanced the resistance of HCC cells to the anticancer effect of Sorafenib (Figure 1D). In addition to the characterization mentioned above, we studied the impact of pyruvate on the ferroptosis in HCC cells for comparative analysis, which is another major metabolite in the glycolysis pathway. Notably, we observed that the pyruvate treatment has caused slight survival improvement in HCC cells incubated with ferroptosis-inducing agents, but the changes were not statistically significant (Figures S1G and S1H). In accordance with the modest

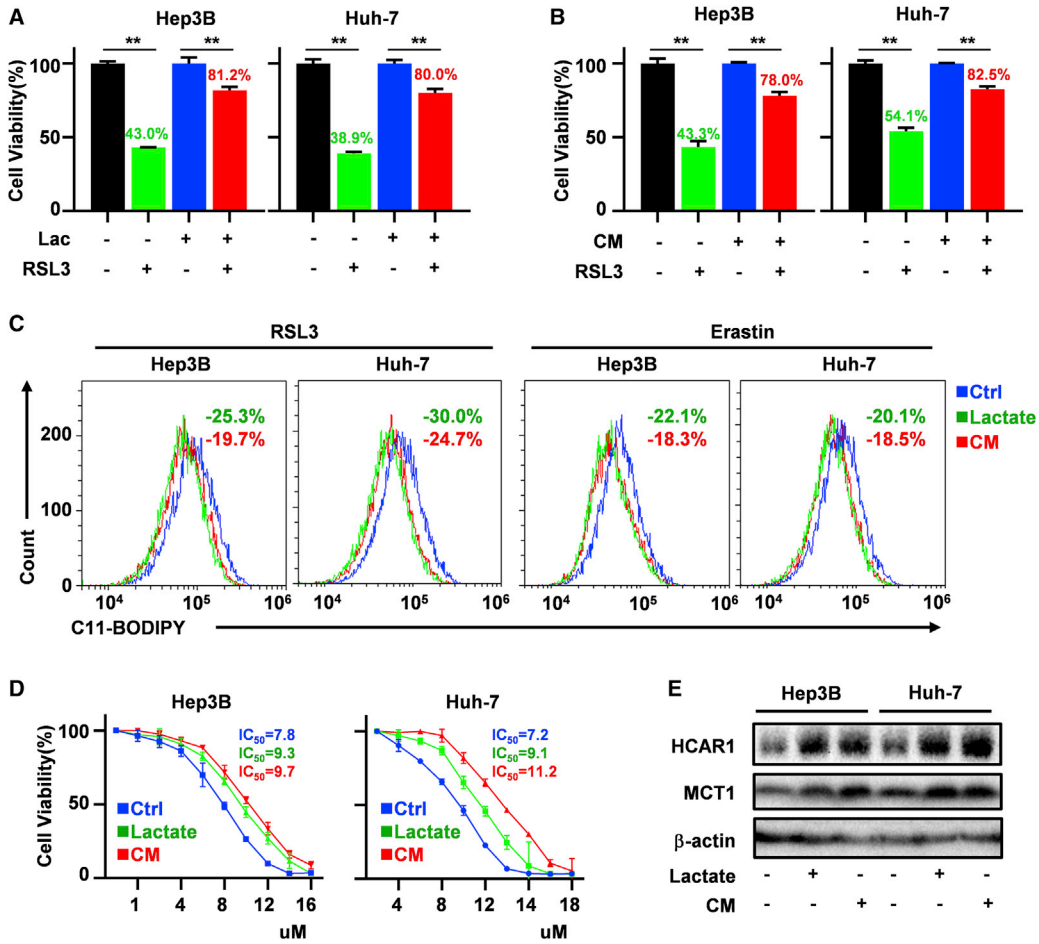

Figure 1. Lactate Rescues HCC Cells from Ferroptosis Induced by RSL3, Erastin, and Sorafenib

(A–E) Changes in the viability (A and B) of liver cancer cells after the treatment with RSL3 (200 nM). Cells were incubated with lactate (20 mM) or CM for 24 h (n = 3), "n" represents the number of cell samples in each group. Changes in the lipid ROS levels (C), Sorafenib resistance (D), and HCAR1/MCT1 expression levels (E) after the incubation with lactate (20 mM) or CM. n = 3, "n" represents the number of cell samples in each group. The significance of difference was determined via Student's t test, **p < 0.01. Data are presented as the mean ± SD.

rescuing effect of pyruvate on ferroptotic HCC cells, it was further detected that the expression levels of HCAR1 and MCT1 in those pyruvate-treated HCC cells showed no obvious changes (Figure S1I), suggesting specific effects of lactate on regulating the ferroptosis response in HCC cells. These observations collectively demonstrate that lactate could protect liver cancer cells from ferroptotic cell death in a specific manner.

The enhanced ferroptosis resistance observed in lactate or CM-treated liver cancer cells mentioned above was further supported by the flow cytometric analysis after C11-BODIPY$^{591/581}$ staining. Specifically, the quantitative analysis showed that RSL3-induced intracellular lipid ROS in Hep3B cells has decreased by 25.3% and 19.7%, respectively, after the incubation with exogenous lactate or CM, while the relative value of decrease for Erastin-treated Hep3B cells after the same treatments was 22.1% and 18.3%, respectively. The decreasing lipid ROS levels due to lactate or CM treatment were also reflected by the increasing half-maximal inhibitory concentration (IC_{50}) values of Sorafenib after different treatments, which increased from 7.8 to 9.3 μM (lactate supplemented) and 9.8 μM (CM) (Figure 1D), respectively. These observations collectively indicated that high lactate level or CM treatment could rescue HCC cells from the ferroptotic damage from ferroptosis inducers by lowering the lipid peroxidation. It was also detected via western blot assay that the treatment of excessive lactate has upregulated the expression levels of HCAR1 and MCT1 (Figure 1E), and the effect was found to be concentration dependent (Figure S1F), which is consistent with the patterns of lactate-induced metabolic rewiring in previous reports (Roland et al., 2014; Xie et al., 2020).

HCAR1 Is Involved in the Emergence of Ferroptosis Resistance in HCC Cells

HCAR1 is the Gi-protein-coupled receptor for lactate and is associated with multiple cancer indications (Brown et al., 2020; Brown and Ganapathy, 2020; Feng et al., 2017), but its role in liver cancers is still not clear. Considering the predominant importance of HCAR1 on the MCT1 in lactate transport and

metabolism (Roland et al., 2014), we then investigated its potential role in regulating the lactate-mediated ferroptosis resistance in liver cancer. By analyzing The Cancer Genome Atlas (TCGA) data, we found that the expression level of HCAR1 has been drastically upregulated in HCC tissues in comparison with the peripheral healthy tissues and that the HCAR1 upregulation is usually associated with poor treatment outcome and terrible prognosis (Figures 2A and 2B). The results from the TCGA database are also consistent with the analysis on tumor tissue samples extracted from patients with HCC and Hep3B/Huh-7 cell lines, which have higher mRNA and protein levels of HCAR1 than normal cells according to qPCR and western blot assays (Figures 2C and 2D; Figures S2A and S2B). Interestingly, we observed that treating HCAR1-interference Huh-7 cells with liproxstatin-1 (Lip-1) only caused modest recovery of cell survival (19.2%) (Figure 2E; Figures S2C–S2E), indicating that HCAR1 knockdown could induce cell death via multiple other pathways in addition to ferroptosis. Meanwhile, knocking down HCAR1 in Huh-7 cells has also enhanced their susceptibility to Sorafenib (Figure 2F) and increased their intracellular lipid ROS levels (27.7%) (Figure 2G) to induce pronounced cell death. Furthermore, we knocked down the HCAR1 in Huh-7-tumor-bearing mice and monitored the tumor progression. The results indicate that the tumor tissues in HCAR1-knockdown mice showed higher lipid ROS levels (27.5%) than the control group (Figures 2H–2I), leading to significant growth inhibition (Figure S2F) and prolonged survival (Figure 2J). It was also observed that the HCAR1 knockdown has downregulated the expression of MCT1 by 85% but did not affect MCT4 (Figure 2K), suggesting the regulatory interactions in between. The Lip-1 could also partially reverse the growth inhibition without affecting the expression level of MCT1. These observations support our hypothesis that HCAR1 and MCT1 are involved in the lactate-dependent ferroptosis resistance in tumor cells.

Blocking the HCAR1/MCT1-Mediated Lactate Import Exacerbates Ferroptosis

After confirming the involvement of the HCAR1 in the regulation of the ferroptosis process, we investigated whether blocking the lactate import could affect the ferroptosis sensitivity of liver cancer cells. Here, we first monitored the changes of lipid ROS after blockading the MCT1-mediated lactate intake using MCT1 small interfering RNA (siMCT1) (Figure S3A) or the MCT1 inhibitor AZD3965 (Huang et al., 2020). C11-BODIPY$^{591/581}$ staining results demonstrated that both treatments could upregulate the lipid ROS levels in Hep3B cells (49.6% for siMCT1 and 43.5% for AZD3965) and Huh-7 cells (32.5% for siMCT1 and 38.5% for AZD3965) (Figures 3A and 3B), leading to a drastic decrease in the survival rate of the liver cancer cells (Figures 3C and 3D). Moreover, the tumor inhibition effect induced by siMCT1 and AZD3965 was found to be positively correlated to the length of the incubation period, presumably due to the time required for the activation of the related biological processes (Figure S3C). Meanwhile, it was observed that the enhanced lipid ROS production and growth inhibition in MCT-1-inhibited liver cancer cells could be rescued by the ferroptosis inhibitor of Lip-1. Markedly, it was observed that the lipid peroxidation capacity of AZD3965 has been significantly reduced in HCAR1-knockdown HCC cells for Hep3B and Huh-7, respectively (Figure S3B), which is supportive of the regulatory effect of HCAR1 on MCT1 expression. Similar to the treatment with siMCT1, the AZD3965-mediated MCT1 inhibition has also elevated the lipid ROS levels in the cancer cells on liver-tumor-bearing mice by 52.8% and induced ferroptosis (Figures 3E–3G), leading to pronounced tumor inhibition and prolonged mouse average survival from 51 to 88.8 days (Figures 3H and 3I). Moreover, the survival benefits by AZD3965 treatment could be partially nullified by the ferroptosis inhibitor of Lip-1, again suggesting the therapeutic potential of HCAR1/MCT1 for ferroptosis-based HCC therapy.

Extracellular Lactate Upregulates the SCD1 Expression in HCC Cells

It is well established that PUFAs and MUFAs are the two major lipids that affect the ferroptosis susceptibility in cancer cells. Specifically, PUFAs are synthesized by ACSL4 and are the preferred substrate for lipid peroxidation, while MUFAs are synthesized by SCD1 and may enhance the ferroptosis resistance in tumor cells by reducing the accumulation of cytotoxic lipid ROS in the cytoplasmic membrane (Das, 2019; Magtanong et al., 2019; Tesfay et al., 2019). Based on the insights discussed above, we first assessed the relationship between MCT1 and ACSL4/SCD1. According to the results extracted from the TCGA database, the expression level of MCT1 is positively correlated to SCD1 but negatively related to ACSL4 (Figures 4A and 4B). The different trends in SCD1 and ACSL4 expression were also supported by the western blot analysis on the HCC tumor specimens extracted from real-life patients (Figure 4C). The lactate-induced changes in SCD1/ACSL4 expression were also examined *in vitro* by monitoring the mRNA and protein levels of SCD1 and ACSL4 in Hep3B and Huh-7 cells, which were incubated with exogenous lactate or the CM. The results collectively demonstrated that HCC cells grown in lactate-supplemented conditions showed upregulated SCD1 expression (446.6% for Hep3B and 294.6% for Huh-7) but downregulated ACSL4 expression (75.6% for Hep3B and 72.0% for Huh-7) at the mRNA level (Figures 4D and 4E) as well as the protein level (Figures 4F and 4G). After inhibiting the MCT1 expression in HCC cells cultured in lactate using siRNA, it was observed that mRNA and protein expressions of SCD1 have both decreased significantly, while those of ACSL4 have increased in a synchronized manner (Figures 4H and 4I). After depleting the MCT1 expression using small hairpin RNAs (shRNAs), we found that lactate supplementation was no longer capable of upregulating the expression of SCD1 or affecting the lipid ROS levels in HCC cells (Figures S4A–S4C). We also used siHCAR1 to inhibit the lactate import in HCC cells, and the results were highly consistent (Figure 4J). However, no obvious changes were observed in the expression levels of other key ferroptosis regulators including fibroblast-specific protein 1 (FSP1) and glutathione peroxidase 4 (GPX4) after lactate supplementation or HCAR1/MCT1 knockdown (Figures S4D–S4G), indicating that the pro-ferroptosis effect of the lactate-blocking treatment was achieved primarily through modulating the intracellular lipid metabolism rather than interfering with those conventional ferroptosis regulators. Considering that SCD1 is the primary enzyme for the

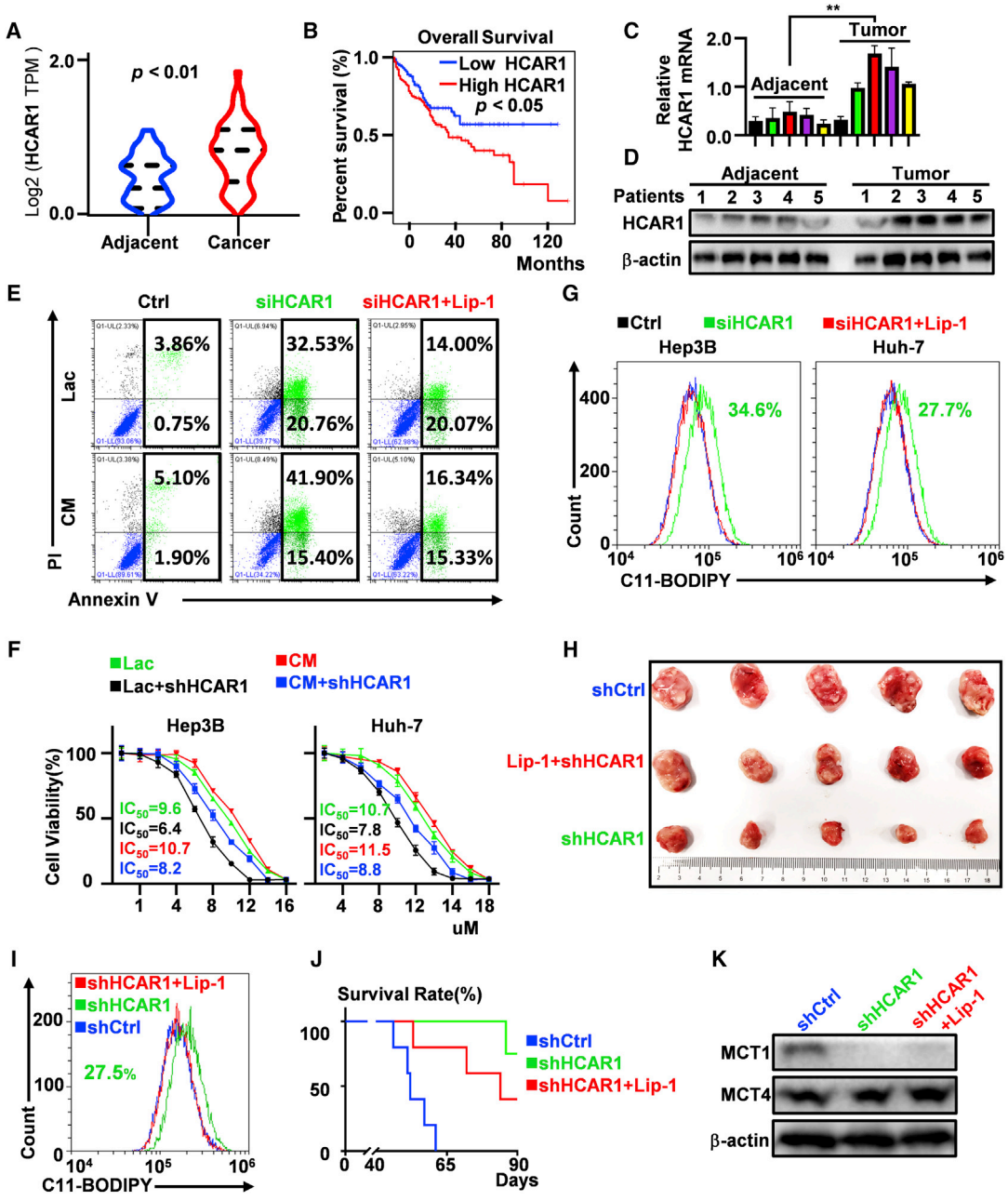

Figure 2. Investigations on the Relationship between HCAR1 and Ferroptosis of HCC Cells

(A) Expression levels of HCAR1 in HCC cells according to the TCGA database (n = 49).

(B) Correlation between HCAR1 expression level and patient prognosis according to the TCGA database (n_{high} = 157, n_{low} = 112), "n" represents the number of data entries.

(C and D) mRNA and protein levels of HCAR1 in the tumor tissue specimen extracted from patients with HCC ($n_{adjacent}$ = n_{tumor} = 5), "n" represents the number of tissue samples.

(E) Flow cytometric analysis on cell viability of liver cancer cell after different treatments.

(F) Changes in the Sorafenib sensitivity in HCC cells cultured in lactate or CM for 24 h after siHCAR1 (100 ng) transfection (n = 3), "n" represents the number of cell samples in each group.

(G) Flow cytometric analysis on the intracellular lipid ROS levels in HCC cells after different treatments.

(H and I) Changes in tumor size (n = 5) and lipid ROS in shHCAR1-treated tumor, "n" represents the number of mice in each group.

(J) Mouse (n = 6) survival after different treatments, "n" represents the number of mice in each group.

(K) The protein expression levels of key lactate transporters after HCAR1 knockdown. The significance of difference was determined via Student's t test, **p < 0.01. Data are presented as the mean ± SD.

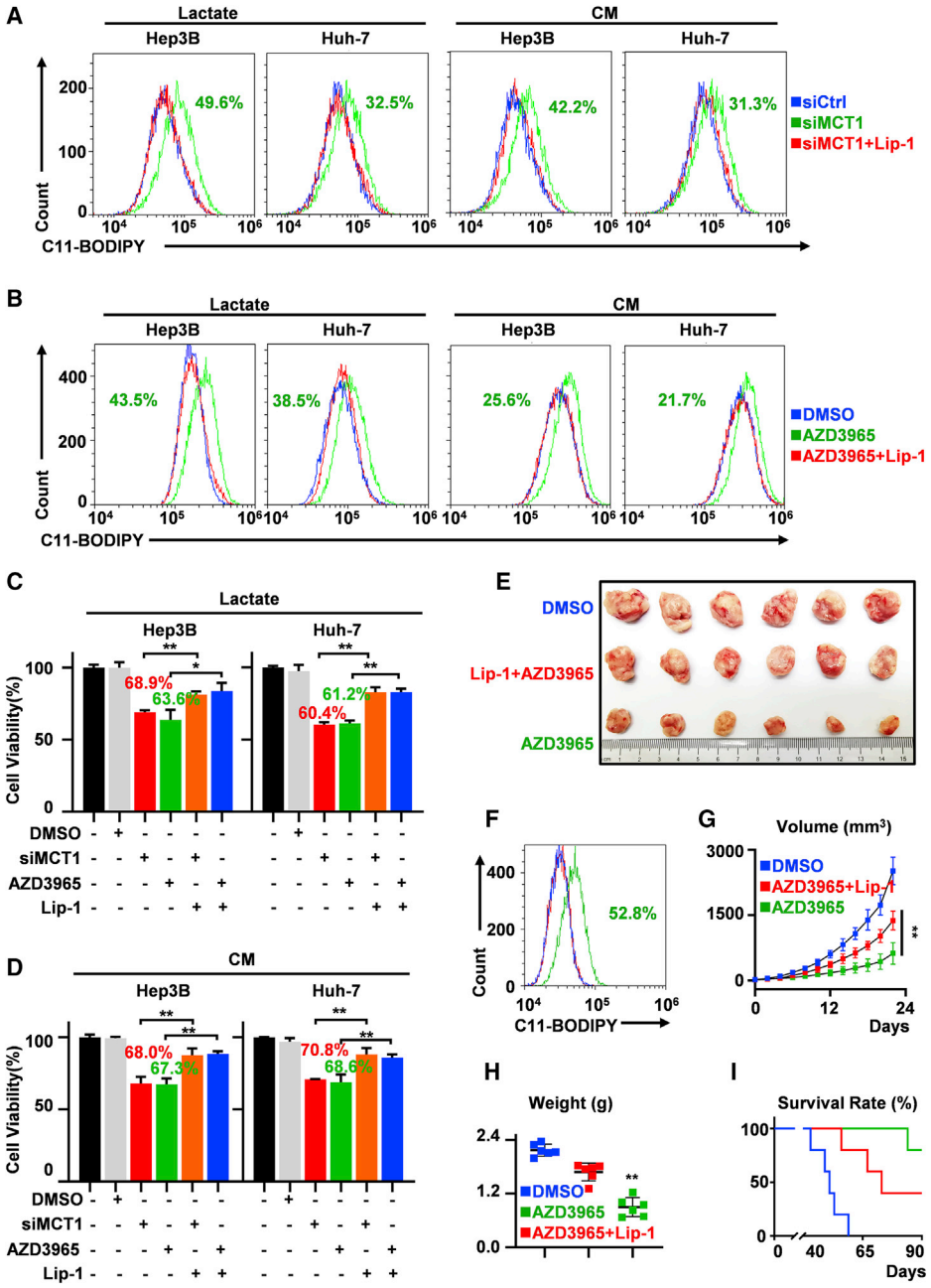

Figure 3. Disrupting the Lactate Import Promotes Ferroptosis in HCC Cells

(A–D) Changes in the lipid ROS levels (A and B) and cell viability (C and D) of HCC cells after the MCT1 inhibition by siRNA (200 ng) (n = 3) or AZD3965(10 nM) treatment for 24 h, "n" represents the number of cell samples in each group.

(E–H) Changes in the size, lipid ROS levels, volume and weight of the tumor tissues on mouse models (n = 6) after the treatment with AZD3965 (50 mg/kg) by oral gavage once every 2 days, "n" represents the number of mice in each group.

(I) Kaplan-Meier survival curve of the tumor-bearing mice (n = 6) after the treatment with AZD3965, "n" represents the number of mice in each group. The significance of difference was determined via Student's t test, *p < 0.05, **p < 0.01. Data are presented as the mean ± SD.

biosynthesis of MUFAs in human body, the results mentioned above are suggestive that lactate-mediated ferroptosis resistance may be associated with SCD1 and the related upstream pathway. Moreover, as the ACSL4-mediated PUFA acylation is a confirmed contributor to ferroptotic cell death (Li et al., 2019), we anticipate that the MCT1-inhibition-induced changes in SCD1 and ACSL4 expression might act in a synergistic manner to alleviate ferroptosis resistance in HCC cells. These observations were further supported by the lipidomic analysis. Specifically, the MCT1 knockdown has caused a significant decrease

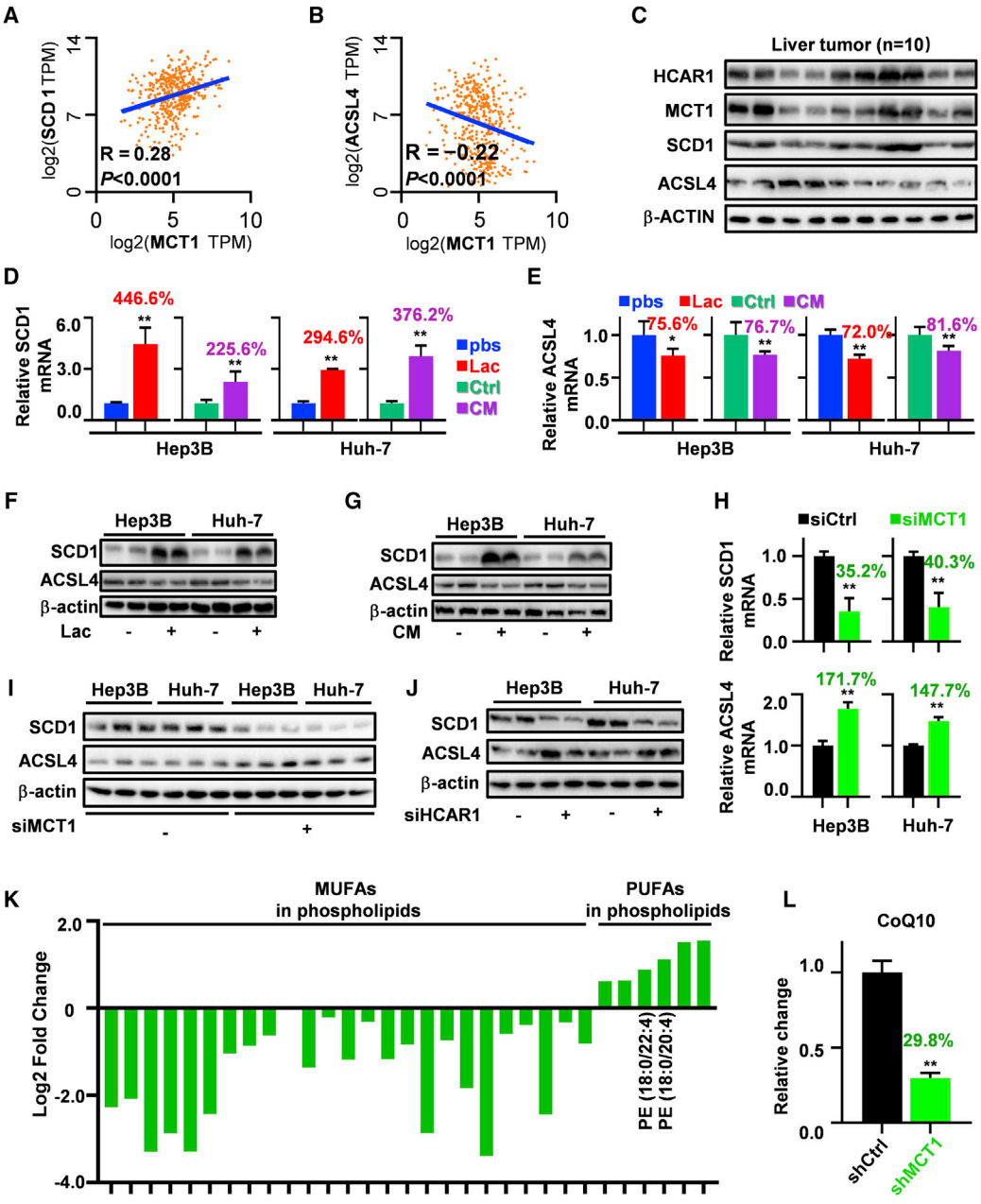

Figure 4. Lactate Import Promotes the Expression of SCD1 in HCC Cells

(A and B) Pearson correlation analysis on the correlation between MCT1/SCD1 and MCT1/ACSL4 according to the TCGA database (n = 424), "n" represents the number of datasets.

(C–L) (C) Western blot analysis on the expression levels of HCAR1, MCT1, SCD1, and ACSL4 in cancer tissue specimens from real-life patients (n = 10), "n" represents the number of patients. (D-G) The changes in the mRNA (D and E) and protein (F and G) expression levels of SCD1 and ACSL4 in lactate or CM-treated Hep3B and Huh-7 cells (n = 3), "n" represents the number of cell samples in each group. (H–I) Changes of the mRNA (n = 3) (H) and protein (I) levels of SCD1 and ACSL4 in Hep3B and Huh-7 cells cultured in lactate after the siMCT1 (200 ng)-mediated MCT1 inhibition, "n" represents the number of cell samples in each group. (J) Changes in the expression levels of SCD1 and ACSL4 in Hep3B and Huh-7 cells cultured in lactate after the treatment by siHCAR1 (100 ng). (K–L) Changes in the phospholipid compositions (K) and CoQ10 (L) in Huh-7 cells after MCT1 knockdown (n = 3), "n" represents the number of cell samples in each group. The significance of difference was determined via Student's t test, *p < 0.05, **p < 0.01. Data are presented as the mean ± SD.

in the production of phospholipids containing MUFAs as well as downregulated the expression of coenzyme Q10 (CoQ10) (Figures 4K and 4L), which is an important enzyme in lipid metabolism and a downstream product of SCD1 (Tesfay et al., 2019), while those of the pro-ferroptosis phosphatidylethanolamine (PE)(18:0/20:4) and PE(18:0/22:4) have increased at

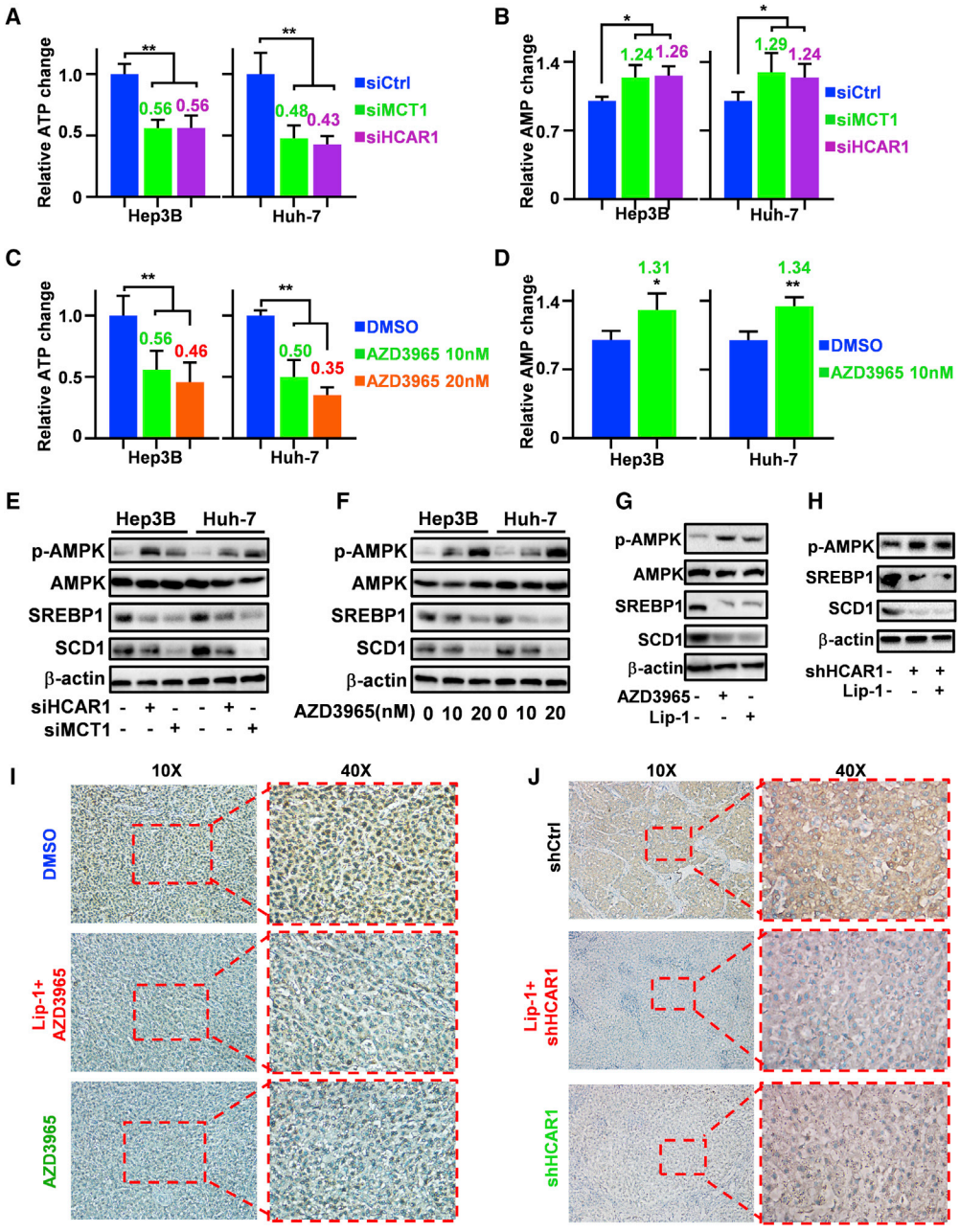

Figure 5. Lactate Upregulates the Expression of SCD1 via AMPK-SREBP1 Pathway

(A–J) Changes in the ATP level (A and C), AMP level (B and D), and key proteins (E and F) in Hep3B and Huh-7 cells after the treatment with siHCAR1 (100 ng), siMCT1 (200 ng), or AZD3965. (G and H) Expression of key proteins in Huh-7 tumor treated with AZD3965 (G) or shHCAR1 (H). (I and J) Immunochemical staining assay on the SCD1 expression in Huh-7 tumor treated with AZD3965 (I) or shHCAR1 (J). The significance of difference was determined via Student's t test, *$p < 0.05$, **$p < 0.01$. Data are presented as the mean ± SD. n = 3, "n" represents the number of replications.

varying degrees (Figure 4K), immediately suggesting the dual-faceted impact of MCT1 inhibition in the biosynthesis of ferroptosis-related lipids in HCC cells.

To confirm whether the intracellular lactate regulate the expression of SCD1 in liver cancer cells, we then investigated the metabolic consequences of lactate import inhibition by measuring the changes in ATP levels. It was observed that all the lactate-blocking treatments (siMCT1, siHCAR1, and AZD3965E) have caused a significant decrease in the ATP levels in HCC cells (56.1%, 56.2%, and 45.8% in Hep3B cells; 47.8%, 42.7%, and 35.2% in Huh-7 cells) (Figures 5A and 5C), while the AMP levels have increased at varying degrees (24%, 26%, and 31% in Hep3B; 29%, 24%, and 34% in Huh-7) (Figures 5B and 5D). By comparison, the AMP:ATP ratio in lactate- and CM-

treated HCC cells has decreased by 73% and 72% in Hep3B cells and by 62% and 60% in Huh-7 cells (Figures S5A and S5B). According to previous insights, increasing the AMP:ATP ratio would activate the AMPK via phosphorylation, which is a cellular energy sensor with major roles in regulating the intracellular lipid metabolism (Han et al., 2019; Pucino et al., 2019). Results from western blot assay indicate that lactate-blockading treatments with siHCAR1, siMCT1, and AZD3965 could upregulate phosphorylated AMPK (p-AMPK) in liver cancer cells, while downregulating the expression of SCD1 via the inhibition of SREBP1 (mature SREBP1) in the AMPK signaling pathway (Figures 5E and 5F). In addition to temporarily silencing HCAR1 and MCT1 expression using siRNAs, we also monitored the changes in key biomarkers after treatment with HCAR1/MCT1-depleting shRNAs (shHCAR1 and shMCT1). As shown by the results, the permanent depletion of HCAR1 and MCT1 in HCC cells would both lead to the upregulation of p-AMPK and the downregulation of the downstream SREBP1 and SCD1 (Figures S5C and S5D). Furthermore, we confirmed the p-AMPK-mediated SCD1 downregulation *in vivo* based on the western blot (Figures 5G and 5H) and immunostaining analysis (Figures 5I and 5J), in which the HCAR1/MCT1 inhibition treatments could activate the p-AMPK to downregulate the expression of SREBP1.

In complement to the mechanistic characterizations mentioned above, we also investigated the regulatory role of SCD1 in the ferroptosis in HCC cells using oleic acid (OA) or palmitoleic acid (POA), which are typical MUFAs in the human body and also the primary catalytic products of SCD1 (Tesfay et al., 2019). It was then detected that the addition of exogenous OA or POA could rescue HCC cells from the proliferation inhibition effect caused by the siHCAR1/siMCT1-induced SCD1 deficiency (Figures 6A and 6B). Markedly, these two downstream metabolites of SCD1 could reduce the generation of the ferroptosis-characteristic lipid ROS in HCAR1/MCT1-depleted HCC cells (Figures 6C and 6D) as well as promote the progression of shHCAR1-treated tumors *in vivo* (Figures 6E–6J), evidently demonstrating the relevance of SCD1-mediated lipid metabolism for ferroptosis regulation. Meanwhile, the expression levels of MCT1 and SCD1 in HCAR1-knockdown tumors remained at the similar level (Figure 6K). Furthermore, we have found that overexpressing HCAR1 in HepG2 cells could upregulate the expression of both MCT1 and SCD1 as well as suppress the generation of lipid ROS in RSL3-treated HCC cells (Figures S6A and S6B). Extending from the results mentioned above, we also monitored the impact of SCD1 overexpression on the cytotoxic effects by siRNA-induced MCT1/HCAR1 depletion and AZD3965-mediated MCT1 inhibition and found that SCD1 overexpression in HCC cells ameliorates the lipid peroxidation induced by siMCT1, siHCAR1, and AZD3965 (Figures S6C and S6D). This evidence collectively demonstrated that the HCAR1/MCT1-mediated lactate uptake could increase the SCD1 expression through the AMPK-SREBP1 pathway and contribute the ferroptosis inhibition in liver cancer cells.

Blocking the Cross-Membrane Lactate Transport Enhances the Sensitivity of HCC Cells to Ferroptosis-Inducing Agents

To investigate the translational potential of lactate influx blockade for ferroptosis sensitization, we subsequently monitored the tumor growth inhibition effect of the combined treatment of AZD3965 and ferroptosis inducers under clinically relevant conditions. As shown in Figures 7A–7C and Figures S7A and S7B, liver cancer cells incubated in lactate or CM showed apparent resistance to the ferroptosis induced by RSL3 and Sorafenib. However, the cell survival rate has dropped significantly when the liver cancer cells were first treated with AZD3965 to shut down the lactate influx before adding RSL3 or Sorafenib. Similarly, the combination of AZD3965 with RSL3 could also promote the ferroptosis-enabled therapeutic efficacy, as it could increase the intracellular lipid ROS levels by 82.5% (Figure 7D). *In vivo* evaluations further demonstrated that the lipid ROS level in the tumor tissues of the AZD3965/RSL3-treated group was 89.3% higher than in the RSL3-only group (Figure 7E), and it was observed that the tumors in the AZD3965/RSL3 group have almost been ablated (Figures 7F and 7G), evidently suggesting the successful reversal of ferroptosis resistance by AZD3965 treatment.

DISCUSSION

Ferroptosis has attracted substantial interest for the development of new anticancer therapies (Badgley et al., 2020; Friedmann Angeli et al., 2019; Liang et al., 2019; Stockwell et al., 2020). However, translational research in this area has been impeded by the elusive understanding regarding key modulators in the ferroptosis process and the underlying regulation mechanisms. Previous insights collectively demonstrate that ferroptosis in the biological environment is regulated by an intricate interplay of various biomolecules and signaling pathways (Bersuker et al., 2019; Brown et al., 2017; Doll et al., 2019; Li et al., 2019; Shin et al., 2018; Wang et al., 2019), which could be exploited to modulate the tumor cell response to ferroptosis-inducing agents for specific purposes. High extracellular lactate level is a characteristic feature universally observed in most tumors (García-Cañaveras et al., 2019; Ippolito et al., 2019a), and by examining the relation between lactate and ferroptosis, we observe that cells with elevated extracellular lactate levels are usually more resistant to the ferroptotic damage induced by typical ferroptosis inducers such as RSL3, Erastin, and Sorafenib. In this study, we report for the first time that lactate contributes to the ferroptosis resistance in HCC tumor cells by activating the AMPK-SREBP1-SCD1 pathway. Inhibiting the lactate receptor HCAR1 or the influx transporter MCT1 could suppress the lactate uptake by HCC cells and promote the antitumor efficacy of ferroptosis-inducing agents thereafter. Therefore, our study may offer new opportunities for the development and implementation of ferroptosis-based tumor therapies.

The intracellular uptake of lactate by cancer cells is primarily achieved via the MCT1 transporter proteins on the cytoplasmic membrane (Khan et al., 2020; Tasdogan et al., 2020), of which the expression level is regulated by the lactate receptor HCAR1 (Roland et al., 2014). The aberrant upregulation of HCAR1 in HCC cells is supported by both the cancer genomics data in the TCGA database and the HCC specimens from real-life patients. As shown in Figure 2, inhibiting the HCAR1 could reduce their resistance to ferroptosis-inducing

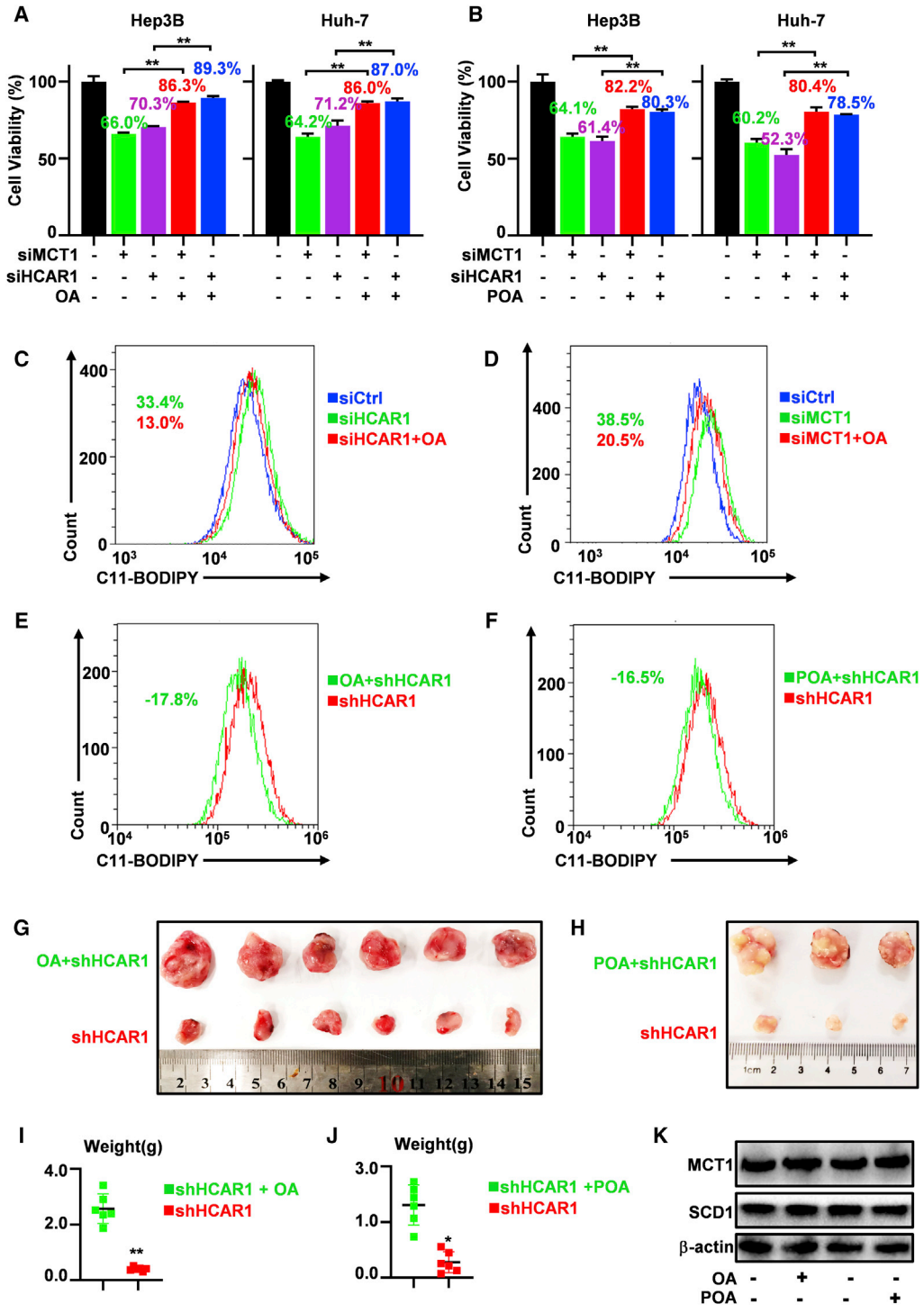

Figure 6. Principle Products of SCD1 (oleic acid [OA], palmitoleic acid [POA]) Are Capable of Reversing the Cytotoxic Damage Induced by HCAR1/MCT1 Inhibition

(A and B) The changes in the survival rate of HCAR1/MCT1-knockdown Hep3B and Huh-7 cells after the treatment with OA (50 μM) (A) or POA (50 μM) (B). n = 3, "n" represents the number of cell samples in each group.

(C and D) Changes in the lipid ROS level in (C) HCAR1- or (D) MCT1-knockdown Huh-7 cells after the treatment with OA (50 μM).

(E–K) Changes of lipid ROS level (E: OA and F :POA), tumor size (G: OA and H: POA), weight (I: OA and J: POA), and (K) protein expression of MCT1 and SCD1 of the HCAR1-knockdown Huh-7 tumors on mouse models after the treatment with OA (n = 6) or POA (n = 6), "n" represents the number of mice in each group. The significance of difference was determined via Student's t test, *p < 0.05, **p < 0.01. Data are presented as the mean ± SD.

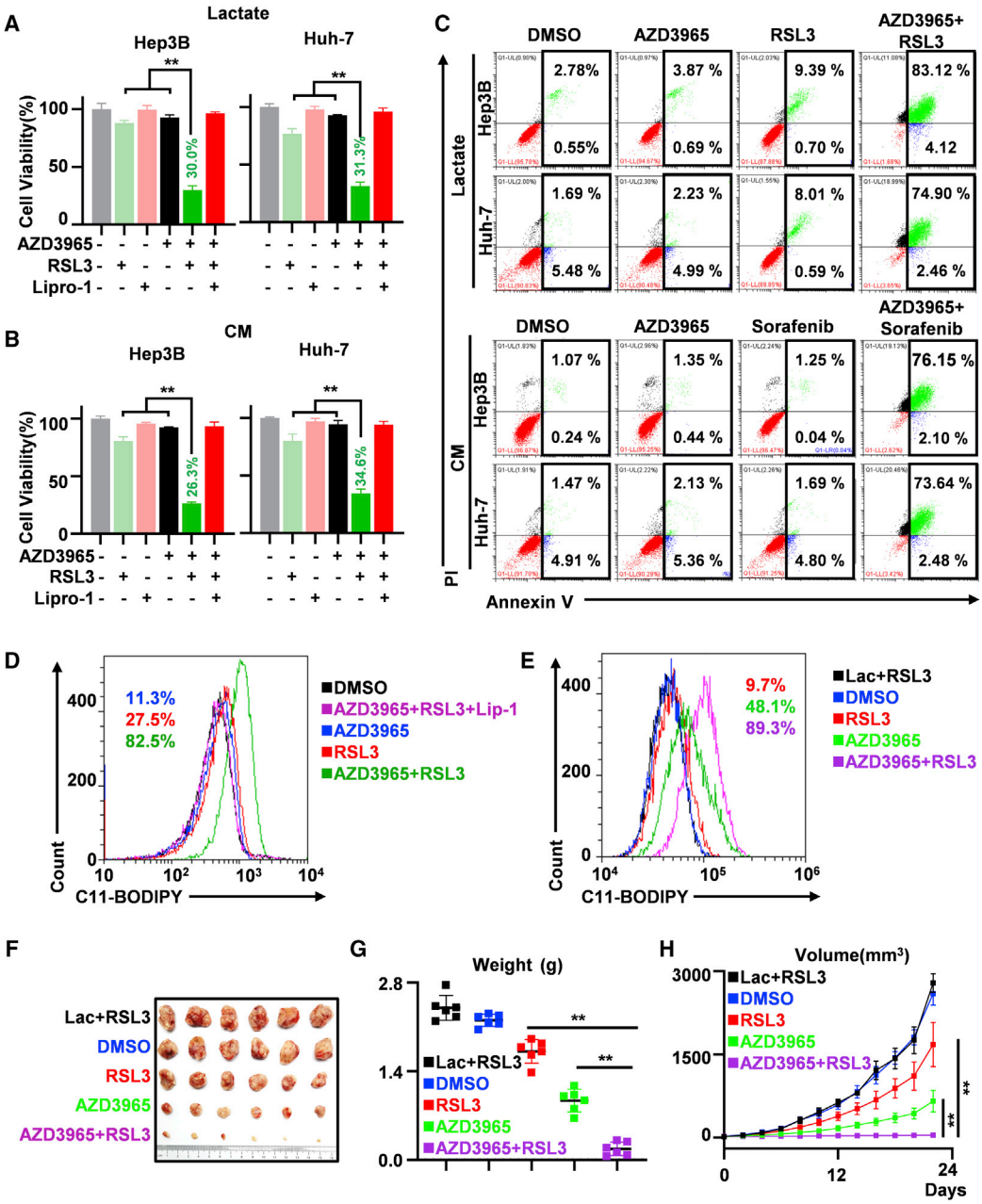

Figure 7. Blocking the Lactate Transport Enhances the Sensitivity of HCC Cells to Ferroptosis Inducers

(A–H) are the survival rates of AZD3965-pretreated (10 nM, 12 h) Hep3B (A) and Huh-7 (B) cells after the incubation with RSL3 (20 nM, 12 h) according to cell viability assay (n = 3), "n" represents the number of cell samples in each group. (C) Survival rate of AZD3965-pretreated Hep3B and Huh-7 cells after the incubation with RSL3 according to flow cytometry. (D) Lipid ROS levels of AZD3965-pretreated Hep3B and Huh-7 cells after the incubation with or without RSL3. (E–H) Lipid ROS level, tumor size, weight, and survival of Huh-7-bearing in mouse models (n = 6) after different treatments, "n" represents the number of mice in each group. The significance of difference was determined via Student's t test, $^{**}p < 0.01$. Data are presented as the mean ± SD.

agents and induce lipid ROS. Meanwhile, treating the HCAR1-inhibited HCC cells with ferroptosis inhibitors such as Lip-1 causes a moderate recovery in the survival rate. The partially rescued ferroptotic cell death suggests that lactate is a negative regulator in the ferroptosis process while also indicating that blocking the lactate transport in liver cancer cells may inhibit their growth and proliferation via some other non-ferroptotic activities. To further determine whether blocking the HCAR1/MCT1-mediated lactate uptake could be used as a supporting treatment to enhance the efficacy of ferroptosis-based therapies against HCC tumors, we inhibit the MCT1 in HCC cells using AZD3965 and monitor the changes in their lipid ROS levels. As expected, the treatment-induced lipid peroxidation and the resultant ferroptotic cell death are

more pronounced in MCT1-inhibited tumors than non-MCT1-inhibited tumors, accompanied with more effective tumor growth inhibition and prolonged survival.

Our mechanistic investigations subsequently demonstrated that the ATP balance in HCC cells has indeed been altered by the excessive extracellular lactate, as L-lactate is capable of supporting the ATP production via the tricarboxylic acid cycle (Hui et al., 2017; Martínez-Reyes and Chandel, 2017). By contrast, blocking the HCAR1/MCT1-mediated lactate uptake via gene knockdown or molecular inhibitors would impede ATP generation, thus increasing the AMP:ATP ratio. The resultant changes in the cellular energy status would initiate the phosphorylation of the AMPK to inhibit the expression of SREBP1 (Bertolio et al., 2019; Han et al., 2019), thus repressing the expression the SCD1 and ameliorating the MUFA-mediated ferroptosis resistance. Consistently, we found that treating the HCAR1/MCT1-inhibted HCC cells with products of SCD1 would render them less susceptible to the ferroptotic effects. The partial recovery of HCC survival was immediate evidence that some other non-ferroptotic cell death mechanisms may be at work, which could be explained by the wide involvement of SCD1 in vital cellular activities, especially apoptosis (Tesfay et al., 2019; Li et al., 2017; Ma et al., 2017). Meanwhile, we also examined the relationship between lactate and ACSL4 and found that lactate could inhibit ACSL4 via other pathways (Brown et al., 2017; Pucino et al., 2019; Xie et al., 2020) and reduce the production of oxidizable PUFAs (Doll et al., 2017; Li et al., 2019). The relative changes in the SCD1 and ACSL4 levels after lactate uptake suggest that the lactate-induced shifting in MUFA and PUFA production may act in concert to synergistically enhance the ferroptosis resistance in HCC cells (Figure 7). These findings collectively demonstrate that lactate could protect HCC cells from ferroptotic cell death in a highly regulated manner as well as validate the therapeutic potential of blocking lactate uptake via HCAR1/MCT1 inhibition for ferroptosis sensitization. This result suggested that the HCAR1/MCT1-mediated lactate import is an ideal therapeutic target for the ferroptosis-based treatment against HCC.

Overall, in this study we demonstrate that the HCAR1/MCT1-mediated lactate uptake is an important factor that accounts for the ferroptosis resistance in HCC cells, which broadens its ability to regulate the ferroptosis activity in tumor cells as well as aid in our understanding in their metabolic and signaling landscape. Meanwhile, our investigations on the ferroptosis response in HCC cells under the combined treatment of HCAR1/MCT1 inhibition and ferroptosis inducers reveals a novel mechanism to sensitize HCC cells for ferroptotic damage, which may contribute to the development of new ferroptosis-based therapies against a wide spectrum of cancer with high lactate indications. Furthermore, it would be interesting to test whether the lactate uptake blockade could be used for the ferroptosis sensitization in other treatment-resistant cancer cells.

STAR★METHODS

Detailed methods are provided in the online version of this paper and include the following:

- KEY RESOURCES TABLE
- RESOURCE AVAILABILITY
  - Lead Contact
  - Materials Availability
  - Data and Code Availability
- EXPERIMENTAL MODEL AND SUBJECT DETAILS
  - Clinical samples
  - Cell line and culturing conditions
  - Mice handling
- METHOD DETAILS
  - Procedures for the incubation with exogenous lactate or pyruvate and CAF-conditioned culture media
  - Q-PCR analysis
  - Immunohistochemistry analysis
  - siRNA Transfections
  - Construction and transfection of plasmid
  - Measurement on cell viability and ATP and AMP levels
  - Western blot analysis
  - Flow cytometeric analysis
  - Lipidomic study
  - TCGA data analysis
  - Animal study
- QUANTIFICATION AND STATISTICAL ANALYSIS

SUPPLEMENTAL INFORMATION

Supplemental Information can be found online at https://doi.org/10.1016/j.celrep.2020.108487.

ACKNOWLEDGMENTS

This work was financially supported by the National Natural Science Foundation of China (11832008, 51773023, 51602034, 51603024), National Key R&D Program of China (2017YFB0702603, 2016YFC1100300), Fundamental Research Funds for the Central Universities (2020CDJQY-A075, 2020CDJYGZL009), Chongqing Outstanding Young Talent Supporting Program (CQYC201905072), Returning Overseas Scholar Innovation Program (CX2018062), and Natural Science Foundation of Chongqing Municipal Government (cstc2018jcyjAX0368, cstc2020jcyj-msxmX0834).

AUTHOR CONTRIBUTIONS

Zhonghong Luo conceptualized this study and designed this project. Youbo Zhao and Menghuan Li performed the major experiments and data analysis. Xueme Yao and Yang Fei assisted in the animal experiments. All authors analyzed the data, discussed the results, and co-wrote the manuscript.

DECLARATION OF INTERESTS

The authors declare no competing interests.

Received: June 14, 2020
Revised: October 10, 2020
Accepted: November 13, 2020
Published: December 8, 2020

REFERENCES

Badgley, M.A., Kremer, D.M., Maurer, H.C., DelGiorno, K.E., Lee, H.J., Purohit, V., Sagalovskiy, I.R., Ma, A., Kapilian, J., Firl, C.E.M., et al. (2020). Cysteine depletion induces pancreatic tumor ferroptosis in mice. Science *368*, 85–89.

Bersuker, K., Hendricks, J.M., Li, Z., Magtanong, L., Ford, B., Tang, P.H., Roberts, M.A., Tong, B., Maimone, T.J., Zoncu, R., et al. (2019). The CoQ oxidoreductase FSP1 acts parallel to GPX4 to inhibit ferroptosis. Nature *575*, 688–692.

Bertolio, R., Napoletano, F., Mano, M., Maurer-Stroh, S., Fantuz, M., Zannini, A., Bicciato, S., Sorrentino, G., and Del Sal, G. (2019). Sterol regulatory element binding protein 1 couples mechanical cues and lipid metabolism. Nat. Commun. *10*, 1326.

Brown, T.P., and Ganapathy, V. (2020). Lactate/GPR81 signaling and proton motive force in cancer: Role in angiogenesis, immune escape, nutrition, and Warburg phenomenon. Pharmacol. Ther. *206*, 107451.

Brown, C.W., Amante, J.J., Goel, H.L., and Mercurio, A.M. (2017). The α6β4 integrin promotes resistance to ferroptosis. J. Cell Biol. *216*, 4287–4297.

Brown, T.P., Bhattacharjee, P., Ramachandran, S., Sivaprakasam, S., Ristic, B., Sikder, M.O.F., and Ganapathy, V. (2020). The lactate receptor GPR81 promotes breast cancer growth via a paracrine mechanism involving antigen-presenting cells in the tumor microenvironment. Oncogene *39*, 3292–3304.

Chen, W., Zheng, R., Baade, P.D., Zhang, S., Zeng, H., Bray, F., Jemal, A., Yu, X.Q., and He, J. (2016a). Cancer statistics in China, 2015. CA Cancer J. Clin. *66*, 115–132.

Chen, Y.J., Mahieu, N.G., Huang, X., Singh, M., Crawford, P.A., Johnson, S.L., Gross, R.W., Schaefer, J., and Patti, G.J. (2016b). Lactate metabolism is associated with mammalian mitochondria. Nat. Chem. Biol. *12*, 937–943.

Conrad, M., and Pratt, D.A. (2019). The chemical basis of ferroptosis. Nat. Chem. Biol. *15*, 1137–1147.

Craig, A.J., von Felden, J., Garcia-Lezana, T., Sarcognato, S., and Villanueva, A. (2020). Tumour evolution in hepatocellular carcinoma. Nat. Rev. Gastroenterol. Hepatol. *17*, 139–152.

Das, U.N. (2019). Saturated Fatty Acids, MUFAs and PUFAs Regulate Ferroptosis. Cell Chem. Biol. *26*, 309–311.

Dixon, S.J., and Stockwell, B.R. (2019). The Hallmarks of Ferroptosis. Annu. Rev. Cancer Biol. *3*, 35–54.

Doll, S., Proneth, B., Tyurina, Y.Y., Panzilius, E., Kobayashi, S., Ingold, I., Irmler, M., Beckers, J., Aichler, M., Walch, A., et al. (2017). ACSL4 dictates ferroptosis sensitivity by shaping cellular lipid composition. Nat. Chem. Biol. *13*, 91–98.

Doll, S., Freitas, F.P., Shah, R., Aldrovandi, M., da Silva, M.C., Ingold, I., Goya Grocin, A., Xavier da Silva, T.N., Panzilius, E., Scheel, C.H., et al. (2019). FSP1 is a glutathione-independent ferroptosis suppressor. Nature *575*, 693–698.

Fang, X., Wang, H., Han, D., Xie, E., Yang, X., Wei, J., Gu, S., Gao, F., Zhu, N., Yin, X., et al. (2019). Ferroptosis as a target for protection against cardiomyopathy. Proc. Natl. Acad. Sci. USA *116*, 2672–2680.

Faubert, B., Li, K.Y., Cai, L., Hensley, C.T., Kim, J., Zacharias, L.G., Yang, C., Do, Q.N., Doucette, S., Burguete, D., et al. (2017). Lactate Metabolism in Human Lung Tumors. Cell *171*, 358–371.e9.

Feng, J., Yang, H., Zhang, Y., Wei, H., Zhu, Z., Zhu, B., Yang, M., Cao, W., Wang, L., and Wu, Z. (2017). Tumor cell-derived lactate induces TAZ-dependent upregulation of PD-L1 through GPR81 in human lung cancer cells. Oncogene *36*, 5829–5839.

Friedmann Angeli, J.P., Krysko, D.V., and Conrad, M. (2019). Ferroptosis at the crossroads of cancer-acquired drug resistance and immune evasion. Nat. Rev. Cancer *19*, 405–414.

García-Cañaveras, J.C., Chen, L., and Rabinowitz, J.D. (2019). The Tumor Metabolic Microenvironment: Lessons from Lactate. Cancer Res. *79*, 3155–3162.

Gaschler, M.M., Andia, A.A., Liu, H., Csuka, J.M., Hurlocker, B., Vaiana, C.A., Heindel, D.W., Zuckerman, D.S., Bos, P.H., Reznik, E., et al. (2018). $FINO_2$ initiates ferroptosis through GPX4 inactivation and iron oxidation. Nat. Chem. Biol. *14*, 507–515.

Han, Y., Hu, Z., Cui, A., Liu, Z., Ma, F., Xue, Y., Liu, Y., Zhang, F., Zhao, Z., Yu, Y., et al. (2019). Post-translational regulation of lipogenesis via AMPK-dependent phosphorylation of insulin-induced gene. Nat. Commun. *10*, 623.

Harmon, C., Robinson, M.W., Hand, F., Almuaili, D., Mentor, K., Houlihan, D.D., Hoti, E., Lynch, L., Geoghegan, J., and O'Farrelly, C. (2019). Lactate-Mediated Acidification of Tumor Microenvironment Induces Apoptosis of Liver-Resident NK Cells in Colorectal Liver Metastasis. Cancer Immunol. Res. *7*, 335–346.

Hassannia, B., Vandenabeele, P., and Vanden Berghe, T. (2019). Targeting Ferroptosis to Iron Out Cancer. Cancer Cell *35*, 830–849.

Huang, T., Feng, Q., Wang, Z., Li, W., Sun, Z., Wilhelm, J., Huang, G., Vo, T., Sumer, B.D., and Gao, J. (2020). Tumor-Targeted Inhibition of Monocarboxylate Transporter 1 Improves T-Cell Immunotherapy of Solid Tumors. Adv. Healthc. Mater., e2000549.

Hui, S., Ghergurovich, J.M., Morscher, R.J., Jang, C., Teng, X., Lu, W., Esparza, L.A., Reya, T., Le Zhan, Yanxiang Guo, J., et al. (2017). Glucose feeds the TCA cycle via circulating lactate. Nature *551*, 115–118.

Ingold, I., Berndt, C., Schmitt, S., Doll, S., Poschmann, G., Buday, K., Roveri, A., Peng, X., Porto Freitas, F., Seibt, T., et al. (2018). Selenium Utilization by GPX4 Is Required to Prevent Hydroperoxide-Induced Ferroptosis. Cell *172*, 409–422 e421.

Ippolito, L., Morandi, A., Giannoni, E., and Chiarugi, P. (2019a). Lactate: A Metabolic Driver in the Tumour Landscape. Trends Biochem. Sci. *44*, 153–166.

Ippolito, L., Morandi, A., Taddei, M.L., Parri, M., Comito, G., Iscaro, A., Raspollini, M.R., Magherini, F., Rapizzi, E., Masquelier, J., et al. (2019b). Cancer-associated fibroblasts promote prostate cancer malignancy via metabolic rewiring and mitochondrial transfer. Oncogene *38*, 5339–5355.

Kanehisa, M., and Goto, S. (2000). KEGG: Kyoto Encyclopedia of Genes and Genomes. Nucleic Acids Res *28*, 27–30.

Khan, A., Valli, E., Lam, H., Scott, D.A., Murray, J., Hanssen, K.M., Eden, G., Gamble, L.D., Pandher, R., Flemming, C.L., et al. (2020). Targeting metabolic activity in high-risk neuroblastoma through Monocarboxylate Transporter 1 (MCT1) inhibition. Oncogene *39*, 3555–3570.

Kim, J., and DeBerardinis, R.J. (2019). Mechanisms and Implications of Metabolic Heterogeneity in Cancer. Cell Metab. *30*, 434–446.

Li, J., Condello, S., Thomes-Pepin, J., Ma, X., Xia, Y., Hurley, T.D., Matei, D., and Cheng, J.X. (2017). Lipid Desaturation Is a Metabolic Marker and Therapeutic Target of Ovarian Cancer Stem Cells. Cell Stem Cell *20*, 303–314 e305.

Li, Y., Feng, D., Wang, Z., Zhao, Y., Sun, R., Tian, D., Liu, D., Zhang, F., Ning, S., Yao, J., and Tian, X. (2019). Ischemia-induced ACSL4 activation contributes to ferroptosis-mediated tissue injury in intestinal ischemia/reperfusion. Cell Death Differ. *26*, 2284–2299.

Liang, C., Zhang, X., Yang, M., and Dong, X. (2019). Recent Progress in Ferroptosis Inducers for Cancer Therapy. Adv. Mater. *31*, e1904197.

Ma, M.K.F., Lau, E.Y.T., Leung, D.H.W., Lo, J., Ho, N.P.Y., Cheng, L.K.W., Ma, S., Lin, C.H., Copland, J.A., Ding, J., et al. (2017). Stearoyl-CoA desaturase regulates sorafenib resistance via modulation of ER stress-induced differentiation. J. Hepatol. *67*, 979–990.

Magtanong, L., Ko, P.J., To, M., Cao, J.Y., Forcina, G.C., Tarangelo, A., Ward, C.C., Cho, K., Patti, G.J., Nomura, D.K., et al. (2019). Exogenous Monounsaturated Fatty Acids Promote a Ferroptosis-Resistant Cell State. Cell Chem. Biol. *26*, 420–432 e429.

Martínez-Reyes, I., and Chandel, N.S. (2017). Waste Not, Want Not: Lactate Oxidation Fuels the TCA Cycle. Cell Metab. *26*, 803–804.

Murphy, M.P. (2018). Metabolic control of ferroptosis in cancer. Nat. Cell Biol. *20*, 1104–1105.

Pucino, V., Certo, M., Bulusu, V., Cucchi, D., Goldmann, K., Pontarini, E., Haas, R., Smith, J., Headland, S.E., Blighe, K., et al. (2019). Lactate Buildup at the Site of Chronic Inflammation Promotes Disease by Inducing $CD4^+$ T Cell Metabolic Rewiring. Cell Metab. *30*, 1055–1074.e8.

Roland, C.L., Arumugam, T., Deng, D., Liu, S.H., Philip, B., Gomez, S., Burns, W.R., Ramachandran, V., Wang, H., Cruz-Monserrate, Z., and Logsdon, C.D. (2014). Cell surface lactate receptor GPR81 is crucial for cancer cell survival. Cancer Res. *74*, 5301–5310.

Shen, Z., Song, J., Yung, B.C., Zhou, Z., Wu, A., and Chen, X. (2018). Emerging Strategies of Cancer Therapy Based on Ferroptosis. Adv. Mater. *30*, e1704007.

Shin, D., Kim, E.H., Lee, J., and Roh, J.L. (2018). Nrf2 inhibition reverses resistance to GPX4 inhibitor-induced ferroptosis in head and neck cancer. Free Radic. Biol. Med. *129*, 454–462.

Siegel, R.L., Miller, K.D., and Jemal, A. (2020). Cancer statistics, 2020. CA Cancer J. Clin. *70*, 7–30.

Song, X., Zhu, S., Chen, P., Hou, W., Wen, Q., Liu, J., Xie, Y., Liu, J., Klionsky, D.J., Kroemer, G., et al. (2018). AMPK-Mediated BECN1 Phosphorylation Promotes Ferroptosis by Directly Blocking System X_c^- Activity. Curr. Biol. *28*, 2388–2399.e5.

Stockwell, B.R., Jiang, X., and Gu, W. (2020). Emerging Mechanisms and Disease Relevance of Ferroptosis. Trends Cell Biol. *30*, 478–490.

Su, S., Chen, J., Yao, H., Liu, J., Yu, S., Lao, L., Wang, M., Luo, M., Xing, Y., Chen, F., et al. (2018). CD10(+)GPR77(+) Cancer-Associated Fibroblasts Promote Cancer Formation and Chemoresistance by Sustaining Cancer Stemness. Cell *172*, 841–856.e816.

Tang, Z., Kang, B., Li, C., Chen, T., and Zhang, Z. (2019). GEPIA2: an enhanced web server for large-scale expression profiling and interactive analysis. Nucleic Acids Res. *47* (*W1*), W556–W560.

Tasdogan, A., Faubert, B., Ramesh, V., Ubellacker, J.M., Shen, B., Solmonson, A., Murphy, M.M., Gu, Z., Gu, W., Martin, M., et al. (2020). Metabolic heterogeneity confers differences in melanoma metastatic potential. Nature *577*, 115–120.

Tauffenberger, A., Fiumelli, H., Almustafa, S., and Magistretti, P.J. (2019). Lactate and pyruvate promote oxidative stress resistance through hormetic ROS signaling. Cell Death Dis. *10*, 653.

Tesfay, L., Paul, B.T., Konstorum, A., Deng, Z., Cox, A.O., Lee, J., Furdui, C.M., Hegde, P., Torti, F.M., and Torti, S.V. (2019). Stearoyl-CoA Desaturase 1 Protects Ovarian Cancer Cells from Ferroptotic Cell Death. Cancer Res. *79*, 5355–5366.

Wang, W., Green, M., Choi, J.E., Gijón, M., Kennedy, P.D., Johnson, J.K., Liao, P., Lang, X., Kryczek, I., Sell, A., et al. (2019). $CD8^+$ T cells regulate tumour ferroptosis during cancer immunotherapy. Nature *569*, 270–274.

Xie, Q., Zhu, Z., He, Y., Zhang, Z., Zhang, Y., Wang, Y., Luo, J., Peng, T., Cheng, F., Gao, J., et al. (2020). A lactate-induced Snail/STAT3 pathway drives GPR81 expression in lung cancer cells. Biochim. Biophys. Acta Mol. Basis Dis. *1866*, 165576.

Zhang, Y., Shi, J., Liu, X., Feng, L., Gong, Z., Koppula, P., Sirohi, K., Li, X., Wei, Y., Lee, H., et al. (2018). BAP1 links metabolic regulation of ferroptosis to tumour suppression. Nat. Cell Biol. *20*, 1181–1192.

Zou, Y., and Schreiber, S.L. (2020). Progress in Understanding Ferroptosis and Challenges in Its Targeting for Therapeutic Benefit. Cell Chem. Biol. *27*, 463–471.

STAR★METHODS

KEY RESOURCES TABLE

REAGENT or RESOURCE	SOURCE	IDENTIFIER
Antibodies		
HCAR1	abcam	Abcam Cat# ab124010, RRID:AB_10976142
GPX4	abcam	Abcam Cat# ab125066, RRID:AB_10973901
ACSL4	abcam	Abcam Cat# ab155282, RRID:AB_2714020
SCD1	CST	Cell Signaling Technology Cat# 2794, RRID:AB_2183099)
SLC7A11	CST	Cell Signaling Technology Cat# 12691, RRID:AB_2687474
pAMPK	CST	Cell Signaling Technology Cat# 2535, RRID:AB_331250
AMPK	CST	Cell Signaling Technology Cat# 5832, RRID:AB_10624867
MCT1	Proteintech	Cat# 20139-1-AP
SREBP1	Proteintech	Proteintech Cat# 14088-1-AP, RRID:AB_2255217
FSP1	Proteintech	Cat# 20886-1-AP
α-SMA	Proteintech	Proteintech Cat# 14395-1-AP, RRID:AB_2223009
Vimentin	Proteintech	Proteintech Cat# 10366-1-AP, RRID:AB_2273020
β-actin	Bioss	Bioss Cat# bs-0061R, RRID:AB_10855480
Biological Samples		
Paraffin liver cancer sections	Chongqing University Cancer Hospital	N/A
Fresh liver biopsy or surgically resected samples	Chongqing University Cancer Hospital	N/A
Chemicals, Peptides, and Recombinant Proteins		
QuickBlock	Beyotime	Cat# P0260
Biotin-labeled Goat Anti-Rabbit	Beyotime	Cat# A0279
HRP-labeled Goat Anti-Rabbit	Beyotime	Cat# A0208
BeyoECL Moon	Beyotime	Cat# P0018FS
PVDF	Millipore	Cat# ISEQ00010
BamHI	NEB	Cat# R0136
EcoRI	NEB	Cat# R3101
pLVshRNA-Puro	Inovogen	Cat# VL3103
pLV-IRES-Puro	Inovogen	Cat# VL3002
siHCAR1	RIBOBIO	Cat# SIGS0000115-1
siMCT1	RIBOBIO	Cat# siB1516103136-1-5
L-lactate	Sigma	Cat# L1750
pyruvate	Sigma	Cat# 107360
sodium lactate	Sigma	Cat# L7022
BODIPY C11	Thermo Fisher	Cat# D3861
Lipofectamine	Thermo Fisher	Cat# L3000015
AZD3965	MCE	Cat# HY-12750
RSL3	MCE	Cat# HY-100218A
Liproxstatin-1	MCE	Cat# HY-12726
Collagenase IV	Thermo Fisher	Cat# 17104019
Dispase II	Sigma	Cat# 4942078001
Critical Commercial Assays		
Annexin V-FITC/PI	BD biosciences	Cat# 556570
Improved Citrate Antigen Retrieval Solution	Beyotime	Cat# P0083

(*Continued on next page*)

Continued

REAGENT or RESOURCE	SOURCE	IDENTIFIER
DAB Horseradish Peroxidase Color Development Kit)	Beyotime	Cat# P0203
Cell Counting Kit-8	Beyotime	Cat# C0038
ATP assay kit	Beyotime	Cat# S0026B
Cell lysis buffer for Western and IP	Beyotime	Cat# P0013
AMP-GLOTM assay kit	Promega	Cat# V5011
FastKing gDNA Dispelling RT SuperMix	Tiangen	Cat# KR118
Q-PCR kit	Tiangen	Cat# FP314
RNAprep pure Cell Kit	Tiangen	Cat# DP430
Experimental Models: Cell Lines		
Hep3B	ATCC	HB-8064
Huh-7	The Cell Bank of Type Culture Collection of Chinese Academy of Sciences	TCHu182
HepG2	ATCC	HB-8065
Experimental Models: Organisms/Strains		
BALB/c	Vital River Laboratory Animal Technology Co., Ltd.	https://buy.vitalriver.com/commodity/detail?productId=4028b2ea69b5248a0169b52627260647 (Identifier: 401)
Oligonucleotides		
Primers for HCAR1, see Table S1	This paper	N/A
Primers for SCD1, see Table S1	This paper	N/A
Primers for ACSL4, see Table S1	This paper	N/A
Primers for GPX4, see Table S1	This paper	N/A
Primers for FSP1, see Table S1	This paper	N/A
shHCAR1 sequence 5′-GCTGCTCATT GTGGCCTTTGT-3′	This paper	N/A
Recombinant DNA		
pLV-shMCT1	This paper	N/A
pEnCMV-SCD1	This paper	N/A
Software and Algorithms		
GraphPad Prism version 8	GraphPad Software	https://www.graphpad.com/scientific-software/prism/
NIS-Elements D	Nikon Corporation	https://www.nikon.com/products/microscope-solutions/support/download/software/imgsfw/#accordion-local-03
CytExpert2.3	Beckman Coulter Life Sciences	https://www.beckman.ae/flow-cytometry/instruments/cytoflex/software
Image Lab Software	Bio-Rad	https://www.bio-rad.com/en-cn/product/image-lab-software?ID=KRE6P5E8Z
iMark Microplate Absorbance Reader	Bio-Rad	https://www.bio-rad.com/en-cn/product/imark-microplate-absorbance-reader?ID=58cca7aa-d943-4e32-9bea-0fe5d140fb9e
real-time PCR	Bio-Rad	CFX384
GEPIA2.0	Tang et al., 2019	http://gepia2.cancer-pku.cn/#index
R	R Core Team	www.r-project.org
KEGG	Kanehisa and Goto, 2000	https://www.kegg.jp/kegg/compound/

RESOURCE AVAILABILITY

Lead Contact

Further information and requests for resources and reagents should be directed to and will be fulfilled by the Lead Contact, Prof. Zhong Luo (luozhong918@cqu.edu.cn).

Materials Availability

All unique/stable reagents generated in this study are available from the Lead Contact with a completed Materials Transfer Agreement.

Data and Code Availability

This study did not generate any unique datasets or code.

EXPERIMENTAL MODEL AND SUBJECT DETAILS

Clinical samples

The liver cancer tissues (n = 10) and peri-tumor tissues (n = 5) were collected from real-life patients in the Chongqing University Cancer Hospital following the corresponding guidelines and policies. The malignant specimens were categorized according to the American Joint Committee on Cancer (AJCC) Cancer Staging Manual 8e, which included Stage II (n = 2), Stage IIIA (n = 5) and IIIB (n = 3). For the HCC samples. 6 patients were male and 4 were female. For the peritumor liver samples, 4 patients were male and 1 patient was female. The average age of the HCC patients was 48 years old.

Cell line and culturing conditions

The cancer associated fibroblasts (CAF) were isolated from the malignant tissues of patients with HCC, the cancer tissues were cut into fragments and digested at 37°C for 2 hours with the buffer comprising collagenase IV (200 U/ml), dispase II (125 μg/mL) and penicillin/streptomycin solution (1%). After filtration with a 70 μm mesh strainer, the supernatant was collected into dishes and cultured in an incubator for 4 hours, and then non-adherent cells were washed off using PBS. in which the expression levels of α-smooth muscle actin (α-SMA: 14395-1-AP, Proteintech) was investigated using immunochemical staining, α-SMA and Vimentin (10366-1-AP, Proteintech) were further detected by flow cytometry. To ensure the phenotypic stability of the CAFs, the cells were subcultured for no more than 15 times. The CAF-conditioned culture media were obtained by incubating CAFs with serum-free medium for 48h. 293T, 7702, HepG2 and Hep3B cells were purchased from ATCC, while Huh-7 cells were purchased from the Cell Bank of Type Culture Collection of Chinese Academy of Sciences. All cells were incubated in recommended culture media at 37°C under a 5%CO_2 atomsphere and were used within 6 months after we received the cell samples.

Mice handling

All animal experiments were carried out strictly following the guidelines of Interim Provisions for the Administration of Laboratory Animals of Chongqing Medical University. Female mice aged around 6-7 weeks were used for this study, which were purchased through Laboratory Animal Center of Chongqing Medical University from Vital River Co. Ltd (Beijing, China). The mice have free access to food and water. After one week, each mouse was injected subcutaneously with 100 μL of Huh-7 cell suspension (5 10^6 units) to establish the tumor model. The mice were grouped randomly, and then subjected to different treatments after subcutaneous tumors became visually detectable. The tumor size was recorded every two days, and the tumor volume was calculated using the formula Volume = (length × width^2)/2. All animals were sacrificed after 3 weeks and tissues were harvested for the following experiments, except for those used in the survival analysis, which were incubated for up to 3 months.

METHOD DETAILS

Procedures for the incubation with exogenous lactate or pyruvate and CAF-conditioned culture media

For the cellular experiments with lactate, the culture media were cultured with L-lactate (Sigma, L1750) or pyruvate (Sigma, 107360) at 20 mmol/L, while the concentration of sodium lactate (Sigma, L7022) in the animal experiments was 1 g/kg. The CAF-conditioned culture media were obtained by incubating CAFs with serum-free medium for 48h. As for the experimental procedures of the *in vitro* characterizations, the relevant cells were first incubated with serum-free DMEM for 12 h and then transferred to the lactate-supplemented media or the CAF-conditioned culture media.

Q-PCR analysis

Total RNA was prepared via using TRIzol (Tiangen, DP430) according to the instructions of manufacturer, the quality of the RNA samples were evaluated via spectrophotometric analysis . These RNAs were subjected to reverse transcription (Tiangen, KR118) with iScript (Bio-Rad Laboratories) to produce cDNA. Q-PCR kit (Tiangen, FP314) was used for real-time PCR (BIORAD, CFX384) to determine the mRNA level relative to beta-actin.

Immunohistochemistry analysis

Tissue samples were fixed in 4% formalin and embedded into paraffin, and then cut into thin sections. The tissue slices were then deparaffinized with xylene and rehydrated them with ethanol, and then treated by antigen (beyotime, P0083) for 20 minutes in a steamer. The endogenous peroxidase was blocked with 4% H_2O_2 and then the samples were treated with QuickBlock(Beyotime, P0260). Primary antibodies of anti-α-SMA (Proteintech, #14395-1-AP, 1:200) and SCD1 (Cell Signaling Technology, #2794. 1;100)

were then added for incubation overnight at 4°C. The samples were then washed and incubated with peroxidase-labeled secondary antibodies (Beyotime, A0279) and 3,3′-diaminobenzidine (Beyotime, P0203) and counterstained with hematoxylin for microscopic examination.

siRNA Transfections

Interferential RNAs were transfected into liver cancer cells with Lipofectamine 3000 (Thermofisher, L3000015). When the confluence reached 70%–80%, cells were transfected with different siRNAs. All short RNAs were purchased from RIBOBIO Biotechnology Co., Ltd (RIBOBIO, siHCAR1: SIGS0000115-1. 100ng; siMCT1: siB1516103136-1-5. 200ng).

Construction and transfection of plasmid

The plasmid for shHCAR1 was constructed based on the pLVshRNA-Puro (Inovogen, VL3103), which was digested by BamHI and EcoRI (NEB, #R0136, #R3101) and inserted with the shHCAR1 sequence (5′-GCTGCTCATTGTGGCCTTTGT-3′). The plasmid for ovHCAR1 was constructed by digesting pLV-IRES-Puro (Inovogen, VL3002) with BamHI and EcoRI to construct pLV-HCAR1-Puro(ovHCAR1) and then inserting HCAR1(NM_032554.4). And pLV-shMCT1 and pEnCMV-SCD1 (NM_005063.5) were constructed by Miaolingbio Ptd Ltd.

The as-prepared constructs (1 μg) were transfected individually in 293T together with 1 μg of packaging constructs (Inovogen, KLV3501 and KLV3502). The supernatant cotaining the lentivirus was then collected and filtered by filter memebrane with a cut-off of 0.45 μm. 500 μL of the lentivirus-containing supernatant was then added into 1 mL of culture medium, which was then transfected into the liver cancer cells with Lipo3000. The expression of shHCAR1, shMCT1, ovSCD1 and ovHCAR1 in liver cancer cells were established after treatment with puromycin (1 mg/mL).

Measurement on cell viability and ATP and AMP levels

The cells were inoculated into a 96 well plate for treatment with different samples. The cells were then processed according to the user manual of Cell Counting Kit-8 (Beyotime, C0038) and the OD values at the wavelength of 450 nm were measured using a microplate reader. Meanwhile, the ATP and AMP levels were determined using ATP assay kit (Beyotime, S0026B) and AMP-GLO^{TM} assay kit (Promega, V5011) according the procedures in the manufacturer's manual. Briefly, around 1 × 10^6 treated cells were washed with cold PBS and then transferred into a 1.5mL centrifugation vail for lysis. The lysate was centrifuged at 10,000 rpm for 5 min, and the supernatant containing ATP and AMP was analyzed with ATP assay kit (Beyotime, S0026B) and AMP-GLOTM assay kit (Promega, V5011).

Western blot analysis

The cell samples were lysed by cell lysate (Beyotime, P0013) and boiled for 10 min to obtain the protein samples, which were then electrophoresed and transferred to polyvinylidene fluoride (PVDF) membrane (Millipore, ISEQ00010). The samples were blocked in 5% non-fat milk for 1 hour at room temperature and then treated with the primary antibodies of HCAR1 (Abcam, ab124010. 1:300), MCT1 (PROTEINTECH, 20139-1-AP. 1:5000), AMPK (Cell Signaling Technology, #5832. 1:1000), p-AMPK (Cell Signaling Technology, #2535. 1:1000), SREBP1 (PROTEINTECH, 14088-1-AP. 1:800), SCD1 (Cell Signaling Technology, #2794. 1:1000), ACSL4 (abcam, #ab155282. 1:5000), GPX4 (abcam, ab125066. 1:1000), FSP1(PROTEINTECH, 20886-1-AP. 1:1000) and β-actin(bioss, bs-0061R. 1:5000), following the standard procedures from manufacturer's instructions. Afterward the samples were incubated with secondary antibadies (Beyotime, A0208) and washed three times. Electrochemiluminescence (Beyotime, P0018FS) was captured on a gel imaging system (Biorad ChemiDoc MP).

Flow cytometeric analysis

To analyze the changes in intracellular lipid ROS levels, the cells were treated with 5 μM BODIPY C11 (Thermo Fisher, D3861) for 30 minutes and then digested with trypsin, and then resuspended in PBS containing 2% FBS. The fluorescence peak of BODIPY C11 would shifted from ~590 nm to ~510 nm, which was used for the subsequent fluorescence imaging.

For the Annexin V-FITC/PI staining of the cell samples, the cells were collected and resuspended in binding buffer (BD biosciences, No. 556570), and then stained with Annexin V-FITC conjugated antibody (5 μL/mL) and propidium iodide (2 μg/mL). The data was collected and analyzed in CytoExpert 2.3.

Lipidomic study

The lipidomic analysis was performed by Metware Ptd Ltd (https://www.metware.cn, Wuhan, China), the processed liver cancer cells were collected according to their instructions and then analyzed using an LC -MS/MS system (SCIEX). The statistics function prcomp R-package (www.r-project.org) was used to carry out the unsupervised principle component analysis (PCA) and the supervised multiple regression orthogonal partial least-squares discriminant analysis (OPLS-DA). In order to avoid overfitting, a permutation test (200 permutations) was performed. The difference in phospholipid compositions between different groups were determind with a absolute Log2 fold change ≥ 1 and a threshold variable importance in the projection (VIP) value (VIP ≥ 1) from the OPLS-DA model. The Student's t test ($p < 0.05$) was used to assess the significance of difference in abundance of metabolites. Identified metabolites were annotated using KEGG Compound database (https://www.kegg.jp/kegg/compound/).

TCGA data analysis

The expression of HCAR1, MCT1, SCD1, ACSL4 and overall survival (OS) were based on the data of The Cancer Genome Atlas (TCGA) (https://www.cancer.gov/). The transcripts per million (TPM) of HCAR1 in adjacent or cancer tissue was log transformed (Log2) and assessed by Student's t test. The OS is analyzed by Kaplan–Meier curve in Gene Expression Profiling Interactive Analysis 2 (GEPIA2.0) webserver (http://gepia2.cancer-pku.cn/#index) (Tang et al., 2019). The Cutoff-High and Cutoff-Low were both set at 50%. To analyze the correlation between MCT1 and SCD1 or ACSL4, we first determined the TPM of MCT1, SCD1, ACSL4 in liver cancer tissue by Log2 mothod, and then the Pearson correlation coefficient between MCT1 (x axis) and SCD1 or ACSL4 (y axis) was calculated in Graphpad prism.

Animal study

All animal experiments were carried out strictly following the guidelines of Interim Provisions for the Administration of Laboratory Animals of Chongqing Medical University.

To investigate the effect of HCAR1 on the ferroptosis of HCC cells in mice, the mice were randomly divided into three groups (n = 5). In the shCtrl group, shCtrl-transfected Huh-7 cells were injected subcutaneously into mice to establish the HCAR1-normal Huh-7 tumors. In the shHCAR1 and Lip1+shHCAR1 group, the shHCAR1-transfected Huh-7 cells were subcutaneously injected into the mice to establish the HCAR1-silenced Huh-7-tumors, while Lip1 was injected intraperitoneally at the dose of 30mg/kg every two days.

To investigate the impact of AZD3965 on the ferroptosis of Huh-7 cells in mice, the mice were randomly divided into three groups (n = 6). In the AZD3965 group, AZD3965 was administered by oral gavage at the dose of 50 mg/kg once every two days. As for the control group, the mice were injected with DMSO. For the Lip-1+AZD3965 group, AZD3965 (50mg/kg) was administered through oral gavage while Lip1 (30mg/kg) was injected intraperitoneally once every two days.

To investigate how OA/POA might affect ferroptosis of Huh-7 cells in mice, HCAR1-knockdown Huh-7 cells were subcutaneously injected into the mice to establish the tumors. Each treatment group comprised 6 mice (n = 6). For the experimental groups, OA or POA were individually injected into abdomen of the tumor-bearing mice at the dose of (50mg/kg), while mice in the control group received no OA/POA injection.

For the evaluation of the tumor inhibition effect of the combinational AZD3965+RSL3 treatment *in vivo*, 5 groups of Huh-7-tumor-bearing mice were established including lactate+RSL3, DMSO, RSL3, AZD3965 and AZD3965+RSL3 (n = 6). Specifically, for the lactate+RSL3 group, the mice were injected with sodium lactate solution (1 g/kg) every day and RSL3 (5 mg/kg) once every two days, respectively. For the DMSO group, DMSO was injected once every two days. As for the RSL3 group, the drug was intratumorally injected into the mice at the dose of 5mg/kg once every two days, while the AZD3965 was administered by oral gavage at the dose of 50 mg/kg once every two days. For those mice that received AZD3965+RSL3 combination treatment, the mice were first treated with AZD3965 via oral gauge on the first day and then intratumorally injected with RSL3 on the next day. The cycle would be repeated once every two days. The tumor size was recorded every two days, and the tumor volume was calculated using the formula Volume = (length × width^2)/2. All animals were sacrificed after 3 weeks and tissues were harvested for the following experiments, except for those used in the survival analysis, which were incubated for up to 3 months.

QUANTIFICATION AND STATISTICAL ANALYSIS

All data were processed in Microsoft Excel and analyzed in GraphPad Prism (GraphPad Prism version 8.0 for Windows) by two-tailed Student's t test. The statistical significance cutoffs were described in figure legends. Results in figures were showed as mean ± sd. The cell viability was detected with iMark^{TM} Microplate Absorbance Reader (Bio-Rad), images were recorded by NIS-Elements D (Nikon). The quantitative C11-BODIPY lipid ROS assay and Annexin V/PI cell viability assay were carried out on CytExpert2.3 (beckman). Pearson's correlation coefficient was used to explore the correlation between variables in the the scatterplots, while the Kaplan-Meier test was used to analyze the mouse survival. The term "n" refers to the number of replicates in the cellular and mouse experiments.